Electrically conductive ZnO/GaN distributed Bragg reflectors grown by hybrid plasma-assisted molecular beam epitaxy

Filip Hjort, Ehsan Hashemi, David Adolph, Tommy Ive, and Åsa Haglund

Photonics Laboratory, Department of Microtechnology and Nanoscience, Chalmers University of Technology, SE-412 96, Gothenburg, Sweden

ABSTRACT

III-nitride-based vertical-cavity surface-emitting lasers have so far used intracavity contacting schemes since electrically conductive distributed Bragg reflectors (DBRs) have been difficult to achieve. A promising material combination for conductive DBRs is ZnO/GaN due to the small conduction band offset and ease of n-type doping. In addition, this combination offers a small lattice mismatch and high refractive index contrast, which could yield a mirror with a broad stopband and a high peak reflectivity using less than 20 DBR-pairs. A crack-free ZnO/GaN DBR was grown by hybrid plasma-assisted molecular beam epitaxy. The ZnO layers were approximately 20 nm thick and had an electron concentration of 1×10^{19} cm^{-3}, while the GaN layers were 80-110 nm thick with an electron concentration of 1.8×10^{18} cm^{-3}. In order to measure the resistance, mesa structures were formed by dry etching through the top 3 DBR-pairs and depositing non-annealed Al contacts on the GaN-layers at the top and next to the mesas. The measured specific series resistance was dominated by the lateral and contact contributions and gave an upper limit of $\sim10^{-3}$ Ω cm^2 for the vertical resistance. Simulations show that the ZnO electron concentration and the cancellation of piezoelectric and spontaneous polarization in strained ZnO have a large impact on the vertical resistance and that it could be orders of magnitudes lower than what was measured. This is the first report on electrically conductive ZnO/GaN DBRs and the upper limit of the resistance reported here is close to the lowest values reported for III-nitride-based DBRs.

Keywords: ZnO, GaN, hybrid PAMBE, DBR, electrical conductivity, VCSEL

1. INTRODUCTION

Vertical-cavity surface-emitting lasers (VCSELs) have several advantages compared to edge-emitting lasers, for instance, low lasing thresholds, small-divergence and circular-symmetric output beams, and they can easily be fabricated in 2D-arrays on a chip and be tested already on the wafer which leads to lower production costs. GaAs-based VCSELs are widely used in short distance optical communication and sensing but the emission wavelength is restricted to the infrared regime which sets a limit for their use. III-nitride based VCSELs, emitting in the ultraviolet and visible spectrum, could open up for new applications in e.g. head-up and near-eye displays, picoprojectors, visible-light communication and bio-medicine.[1,2] The progress of GaN-based VCSELs has been hampered by difficulties relating to growing low resistivity p-GaN, large lattice mismatch, and strong spontaneous and piezoelectric polarization fields in III-nitrides. Despite this, there have lately been several groups reporting on electrically injected GaN-based VCSELs[3–12] but further improvement is still needed in terms of lowering the threshold current density, increasing the output power and improving thermal stability.

In almost all these reports the n-side distributed Bragg reflectors (DBRs) are electrically insulating using either dielectric or epitaxial nitride-based materials. The dielectric DBRs are superior in terms of optical reflectivity but they require complex substrate removal processing or epitaxial lateral overgrowth and generally have poor thermal conductivity. For an n-side epitaxial DBR, the rest of the cavity can be grown monolithically on the bottom DBR, which dramatically improves the heat dissipation. However, in contrast to the AlGaAs material system, there is unfortunately no III-nitride material combination which simultaneously offers high refractive index contrast and small in-plane lattice mismatch. High Al-composition Al(Ga)N/GaN suffer from large lattice

(Send correspondence to Filip Hjort)
E-mail: filip.hjort@chalmers.se, Telephone: +46 31 772 6742

Gallium Nitride Materials and Devices XII, edited by Jen-Inn Chyi, Hiroshi Fujioka, Hadis Morkoç, Yasushi Nanishi, Ulrich T. Schwarz, Jong-In Shim, Proc. of SPIE Vol. 10104, 1010413
 · doi: 10.1117/12.2250126

mismatch (2.5% for AlN/GaN),[13] which can lead to crack formation, while low Al content yields a small index contrast resulting in a narrow stopband width and a demand for many DBR pairs to reach high peak reflectivity. $Al_{0.82}In_{0.18}N$/GaN is a lattice-matched alternative but also suffers from a small index contrast. Despite these challenges, crack-free and high reflectivity DBRs using both AlN/GaN[3,8,14,15] and AlInN/GaN[6,11,16,17] have been successfully grown and used as n-side DBRs in III-nitride VCSELs.

Furthermore, electrically conductive n-type nitride-based DBRs are difficult to realize as the current transport is limited due to the large conduction band offsets, large polarization charges at the interfaces when grown along the c-axis, and low electrical conductivity of AlGaN. Thus, most GaN-based VCSELs have used intracavity contact schemes, enforcing long cavity lengths to reduce lateral resistance. As a result, the longitudinal confinement factor is low and the thick n-doped cavity leads to an overall high optical absorption. To be able to place the contact outside the cavity, on the bottom of the n-side DBR, an electrically conductive DBR should preferably have a specific series resistance below roughly $10^{-3}\ \Omega\,\mathrm{cm}^2$ (corresponding to a 10 Ω resistance for a mesa diameter of 100 μm). In addition, the peak reflectivity has to be above 99%. There are a few reports on electrically conductive Al(Ga)N/GaN DBRs, but their specific series resistances, extracted from IV-characteristics, is in the order of $0.1\ \Omega\,\mathrm{cm}^2$ or above.[18–20] The only exception is the recent demonstration of an $Al_{0.12}Ga_{0.88}N$/GaN DBR by Liu et al.,[21] where the DBR had a specific series resistance of $2 \times 10^{-4}\ \Omega\,\mathrm{cm}^2$. However, due to the low Al-composition the stopband width was as narrow as 11 nm and 40 mirror pairs only resulted in a peak reflectivity of 92% at 368 nm. The lowest reported specific series resistance for an n-type III-nitride-based DBRs is by Meijo University. They demonstrated an n-doped AlInN/GaN DBR with a specific series resistance corresponding to $7.8 \times 10^{-4}\ \Omega\,\mathrm{cm}^2$ for 40 mirror pairs, a peak reflectivity of 99.9% at 404 nm, and a stopband width of 22 nm.[22] The DBR was integrated into a VCSEL[11] and it is to date the only report on III-nitride VCSELs without an intracavity n-contact by using electrically conductive DBRs.

Recently, we demonstrated ZnO/GaN DBRs grown by plasma-assisted molecular beam epitaxy (PAMBE).[23] This could be an alternative to pure III-nitride epitaxial DBRs as the ZnO/GaN combination has a similarly high refractive index contrast as that of AlN/GaN[24,25] but a smaller lattice mismatch (1.9%).[13,26] The material combination is also promising for n-type conductive DBRs because of the very small conduction band offset (∼0.2 eV)[27] and as it for ZnO, in contrast to for AlN, is easy to achieve high electron concentrations.[28] In addition, the spontaneous and piezoelectric polarization partly cancels along the c-direction in metal-polar ZnO/GaN DBRs having strained ZnO, as shown in Sec. 4, resulting in a significant increase in the electrical conductivity. In this work, we investigate the vertical electrical conductivity of PAMBE grown ZnO/GaN DBRs through I-V measurements and simulations.

2. GROWTH

An n-type ZnO/GaN DBR with 5.5 mirror pairs was grown crack-free by hybrid PAMBE, i.e. both materials were grown in the same chamber. A two-temperature growth scheme was used for each material. For more details on the growth see Ref. 23. The root-mean-square surface roughness of the 5.5 pair DBR, determined by AFM, was 2.1 nm. The ZnO layers were roughly 20 nm thick, Zn-polar, and had an electron concentration, determined by Hall measurements on single layers, of approximately $1\times10^{19}\ \mathrm{cm}^{-3}$. The GaN layers were Ga-polar and 80-110 nm thick with an electron concentration of $1.8\times10^{18}\ \mathrm{cm}^{-3}$. The large deviations from the target layer thicknesses of 46 nm for GaN and 56 nm for ZnO, needed to achieve a peak reflectivity at 450 nm, were due to an unstable Zn-source and additional GaN growth during temperature ramps.

Figure 1 shows the reflectance spectrum for the DBR measured with a spot size of a few millimeters. The low peak reflectance can be explained by the layer thickness deviations and Ga-droplets on the surface which originated from Ga-rich growth conditions. A cross-sectional view of the top three mirrors pairs that were electrically characterized is shown in the scanning electron microscope (SEM) image in Fig. 2a. The topmost GaN layer is only approximately 30 nm thick, since substrate heater issues led to an early stop in the growth. The reciprocal space map for the asymmetric $(10\bar{1}5)$ reflection measured by x-ray diffraction (XRD) is presented in Fig. 3 and shows that the ZnO is strained to the GaN. The importance of this aspect on the electrical properties are further discussed in Sec. 4.

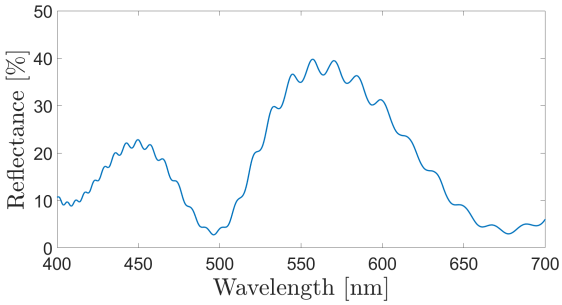

Figure 1. Measured reflectance spectrum of the 5.5 pair ZnO/GaN DBR.

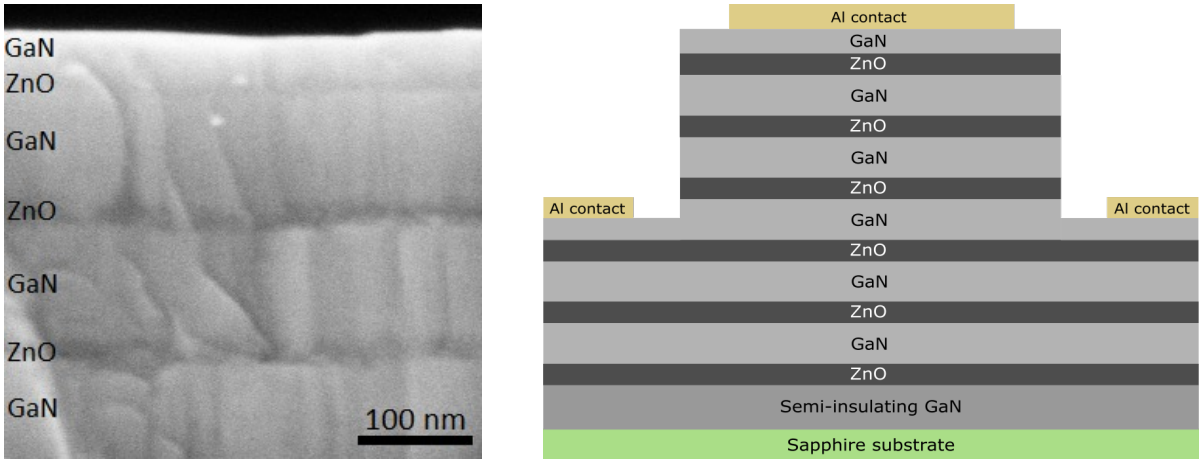

(a) (b)

Figure 2. (a) Scanning electron microscope image of the top three ZnO/GaN DBR pairs. The dark areas correspond to the ZnO and the bright areas to GaN. (b) Schematic figure of a ZnO/GaN DBR mesa with top and bottom Al contacts.

3. ELECTRICAL CHARACTERIZATION

In order to measure the vertical DBR resistance, mesa structures were etched and contacted as can be seen in Fig. 2b. Mesas with 30, 45, 50, 75 and 100 μm radii were formed by Cl_2/Ar inductively coupled plasma reactive ion etching (ICP-RIE) the top 3 DBR-pairs. The etch time was 1 minute using 250 W ICP power, 250 W electrode RF power, 10 mTorr pressure, 30 sccm Cl_2 and 15 sccm Ar flow. By SEM inspection of the DBR cross-section, the etch was verified to have stopped in the GaN layer seen in the bottom of Fig. 2a. 150 nm thick aluminum contacts were deposited by e-beam evaporation at the top and next to the mesas with a lateral distance of 10 μm between the mesa and the top and bottom contact edges. I-V measurements of Al transmission line method (TLM) patterns showed ohmic behavior for as-deposited contacts with a specific contact resistivity of $\sim 10^{-4}\ \Omega\,\mathrm{cm}^2$. The sheet resistance of the DBR was $\sim$200 Ω/sq.

Figure 4 shows the I-V characteristics measured through the top 3 DBR pairs for different mesa radii. From the I-V characteristics, the specific series resistance, R_sA, where A is the mesa area, was calculated and is plotted in Fig. 5. The error bars are calculated from the variations in resistance between mesas with the same radius but at different locations on the sample. Shown in the figure is also the lateral and contact resistance contribution, estimated from TLM measurements. If the vertical resistance of the 3 DBR pairs would be dominating the overall measured resistance, the specific series resistance should be independent of mesa radius, assuming a radially uniform current density across the mesa. This is not the case in Fig. 5, where the specific series resistance increases approximately linear with radius, revealing that the lateral and contact resistances were dominating the measured resistance. This is further confirmed by the estimation of the contribution from lateral and contact resistance shown in the figure. Thus, this only allowed for an estimation of an upper limit for the DBR specific

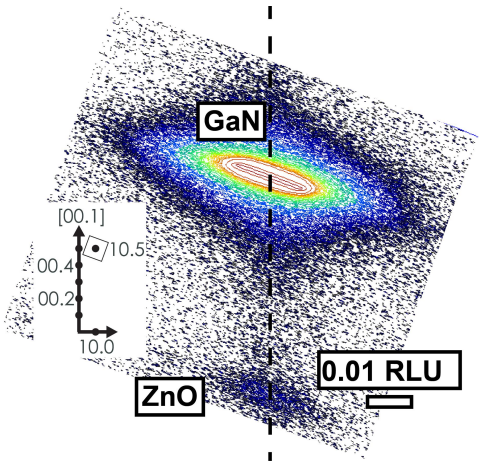

Figure 3. Reciprocal space map for the asymmetric $(10\bar{1}5)$ reflection of the 5.5 pair ZnO/GaN DBR. The dashed line marks the position of the GaN $(10\bar{1}5)$ reflection.

series resistance of $\sim 10^{-3}\ \Omega\,\mathrm{cm}^2$ for 3 pairs. Still, this is comparably low, corresponding to a specific series resistance of less than $7 \times 10^{-3}\ \Omega\,\mathrm{cm}^2$ for a full 20 pair DBR and thus a resistance well below 100 Ω for a 20 pair 100 μm diameter mesa. To investigate if GaN droplets on the surface had any impact on the resistance, small mesa sizes of radius 7.5 μm, which were droplet free, were also explored. The I-V measurements revealed a specific series resistance of about $10^{-3}\ \Omega\,\mathrm{cm}^2$, again limited by lateral and contact resistance, which verifies that the droplets did not affect the vertical resistance.

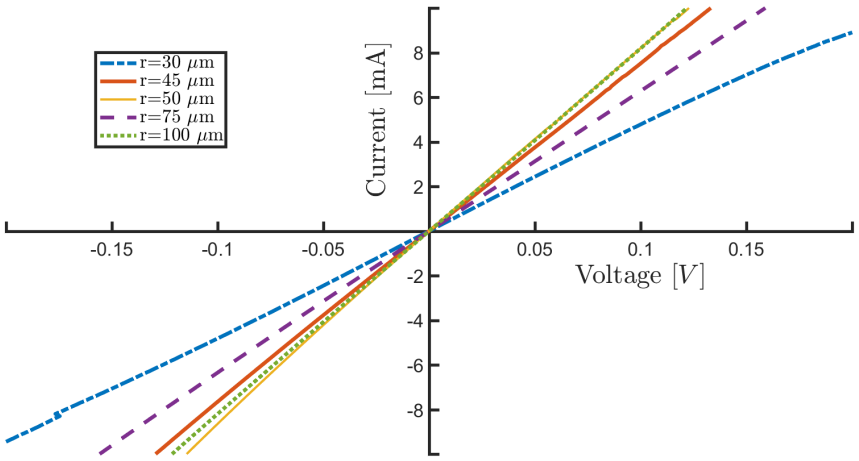

Figure 4. I-V characteristics through 3 DBR pairs of ZnO/GaN for different mesa radii, r.

4. ELECTRICAL SIMULATIONS

To explore the current transport in ZnO/GaN DBRs in greater detail, drift-diffusion simulations were performed using Sentaurus TCAD from Synopsys which self-consistently solved the Poisson and carrier continuity equations and accounted for electron barrier tunneling. The simulated structure consisted of 3 DBR pairs with 80 nm thick GaN and 20 nm thick ZnO layers, and a top 30 nm thick GaN layer, corresponding to what is seen in Fig. 2a. The DBR stack was sandwiched between two ideal ohmic contacts used to control the boundary condition for voltage biased current flow simulations. Simulations of DBRs with target GaN and ZnO thicknesses of 46 and 56 nm, respectively, were also performed. Only a relatively small change in the current flow was seen, indicating that

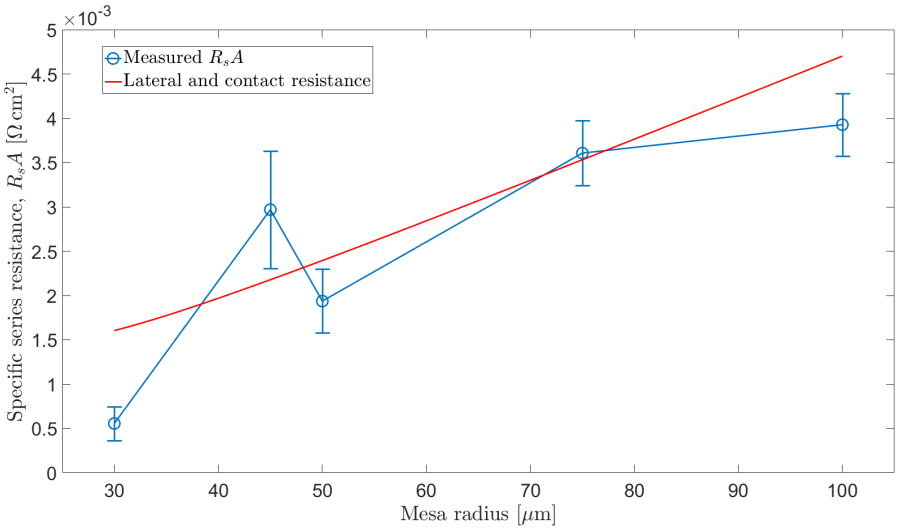

Figure 5. Mean specific series resistance with error bars and the estimated contribution from the lateral and contact resistance as a function of mesa radius.

DBRs with target thicknesses should exhibit similar I-V characteristics as our grown sample. The piezoelectric and spontaneous polarization were accounted for by adding an interface sheet charge density according to[29]

$$\sigma = P_{\mathrm{sp}}^{\mathrm{ZnO}} - P_{\mathrm{sp}}^{\mathrm{GaN}} + 2\left(e_{31} - \frac{c_{13}}{c_{33}}e_{33}\right)\frac{a_{\mathrm{GaN}} - a_{\mathrm{ZnO}}}{a_{\mathrm{ZnO}}}, \tag{1}$$

where e_{13} and e_{33} are piezoelectric constants for ZnO, c_{13} and c_{33} are elastic constants for ZnO, a_{ZnO} and a_{GaN} are the in-plane lattice constants, and $P_{\mathrm{sp}}^{\mathrm{ZnO}}$ and $P_{\mathrm{sp}}^{\mathrm{GaN}}$ the spontaneous polarization charge densities for respective material. Equation (1) describes the sheet charge density for ZnO strained to GaN at the Zn-polar/N-polar interfaces, i.e. at the transition from ZnO to GaN when moving in the [0001] direction of the metal-polar DBR. For the O-polar/Ga-polar interfaces the sheet charge density change sign. Table 1 summarizes the material parameter values used for ZnO and GaN, together with material parameter values for AlN.

Table 1. In-plane lattice constant, a, spontaneous polarization charge density, P_{sp}, piezoelectric constants, e_{31} and e_{33}, and elastic constants, c_{13} and c_{33}, for wurtzite ZnO, GaN, and AlN.[13,26,30,31]

Material	a [Å]	P_{sp} [C/m^2]	e_{31} [C/m^2]	e_{33} [C/m^2]	c_{13} [GPa]	c_{33} [GPa]
ZnO	3.25	-0.057	-0.51	0.89	105	211
GaN	3.19	-0.029	-0.49	0.73	106	398
AlN	3.11	-0.081	-0.60	1.46	108	373

Figure 6 shows the conduction band diagram for relaxed ZnO (no piezoelectric charge) and ZnO fully strained to GaN for two different ZnO electron concentrations of 10^{18} cm^{-3} and 10^{19} cm^{-3}. The electron concentration in GaN was assumed to be 1.8×10^{18} cm^{-3} as determined by Hall measurements. As shown in the figure, the fully strained ZnO yields a considerably lower barrier height at the Zn-polar/N-polar interface compared to relaxed ZnO. This is due to the counteracting contributions to the polarization sheet charge density from spontaneous and piezoelectric polarization caused by the in-plane compressively strained ZnO. Equation (1) and Tab. 1 can be used to calculate the polarization sheet charge density, which yield 0.0072 C/m^2 for ZnO strained to GaN and -0.028 C/m^2 for relaxed ZnO. It should be noted that a similar cancellation would also occur for a strain-compensated state, where ZnO and GaN are strained to an intermediate in-plane lattice constant. For Al(Ga)N/GaN interfaces, the spontaneous and piezoelectric polarization fields point in the same direction due

to the in-plane tensile strained AlN, which leads to a large polarization sheet charge density of -0.10 C/m^2 for AlN strained to GaN, and thus a large potential barrier height. A high carrier concentration can compensate the polarization sheet charges at the interfaces and reduce the potential barrier height. This is shown in Fig. 6 where the strong dependence on carrier concentration is clearly visible. The specific series resistance, extracted from simulated I-V characteristics, is plotted in Fig. 7. It clearly shows the strong dependence of the resistance on both strain and electron concentration in the ZnO layer. Although not presented here, a high doping of the GaN layer leads to a similar reduction of the resistance. Note that the simulated specific series resistance for an electron concentration of 10^{19} cm^{-3} is orders of magnitude lower than the measured values for our 3 DBR pairs, yet another indication of that the lateral and contact resistance is dominating. Thus, the actual specific series resistance of the ZnO/GaN DBR is much lower than what could be measured.

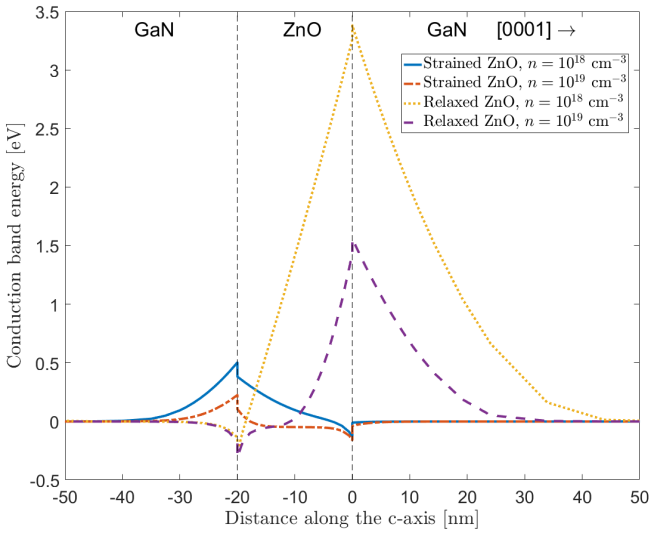

Figure 6. Calculated conduction band diagram of a ZnO/GaN DBR pair for strained and relaxed ZnO and two different electron concentrations. The arrow indicates the growth direction along the c-axis.

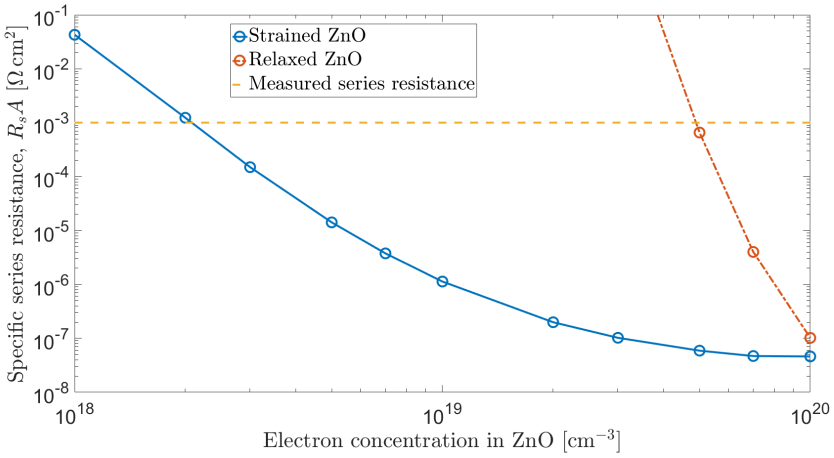

Figure 7. Simulated specific series resistance of three ZnO/GaN DBR pairs as a function of the electron concentration in ZnO for strained and relaxed ZnO. The dashed line indicates the lateral and contact resistance dominated specific series resistance estimated from IV measurements on the ZnO/GaN DBR.

5. CONCLUSIONS

We have, for the first time, demonstrated an electrically conductive ZnO/GaN DBR grown by hybrid PAMBE. The specific series resistance, R_sA, was determined from I-V measurements to be less than $\sim 10^{-3}\ \Omega\,\mathrm{cm}^2$ for 3 DBR pairs. This is close to the lowest values reported for III-nitride-based DBRs.[11,22] However, the total resistance was dominated by lateral and contact resistance, and simulations suggest that the actual vertical specific series resistance of the ZnO/GaN DBR could be orders of magnitudes lower. Simulations further show that the cancellation of the piezoelectric and spontaneous polarization for strained ZnO, and high electron concentrations in ZnO, can greatly reduce the specific series resistance of ZnO/GaN DBRs.

The great potential of n-conductive ZnO/GaN DBRs becomes even more evident when considering that the structure investigated here is unintentionally doped and that both GaN and ZnO[28] can easily be n-doped to high levels. In addition, by further optimizing the growth, both the optical and electrical performance should be improved. The large refractive index contrast, small conduction band offset, ease of n-type doping, comparably small lattice mismatch, and the cancellation of charges induced by piezoelectric and spontaneous polarization, make ZnO/GaN DBRs a very promising alternative to pure III-nitride n-doped DBRs in GaN-based VCSELs.

ACKNOWLEDGMENTS

We would like to thank Hans Hjelmgren from the Microwave Electronics Laboratory, Department of Microtechnology and Nanoscience at Chalmers University of Technology for his support with electrical simulations. This work was funded by the Swedish Research Council, the Swedish Foundation for Strategic Research, The Swedish Energy Agency, and the Department of Microtechnology and Nanoscience at Chalmers University of Technology.

REFERENCES

[1] Feezell, D. F., "Status and future of GaN-based vertical-cavity surface-emitting lasers," *Proc. SPIE* **9363**, 93631G–93631G–13 (2015).

[2] Haglund, A., Hashemi, E., Bengtsson, J., Gustavsson, J., Stattin, M., Calciati, M., and Goano, M., "Progress and challenges in electrically pumped GaN-based VCSELs," *Proc. SPIE* **9892**, 98920Y–98920Y–20 (2016).

[3] Lu, T.-C., Kao, C.-C., Kuo, H.-C., Huang, G.-S., and Wang, S.-C., "CW lasing of current injection blue GaN-based vertical cavity surface emitting laser," *Applied Physics Letters* **92**(14), 141102 (2008).

[4] Higuchi, Y., Omae, K., Matsumura, H., and Mukai, T., "Room-temperature CW lasing of a GaN-based vertical-cavity surface-emitting laser by current injection," *Applied Physics Express* **1**(12), 121102 (2008).

[5] Kasahara, D., Morita, D., Kosugi, T., Nakagawa, K., Kawamata, J., Higuchi, Y., Matsumura, H., and Mukai, T., "Demonstration of blue and green GaN-based vertical-cavity surface-emitting lasers by current injection at room temperature," *Applied Physics Express* **4**(7), 072103 (2011).

[6] Cosendey, G., Castiglia, A., Rossbach, G., Carlin, J.-F., and Grandjean, N., "Blue monolithic AlInN-based vertical cavity surface emitting laser diode on free-standing GaN substrate," *Applied Physics Letters* **101**(15), 151113 (2012).

[7] Onishi, T., Imafuji, O., Nagamatsu, K., Kawaguchi, M., Yamanaka, K., and Takigawa, S., "Continuous wave operation of GaN vertical cavity surface emitting lasers at room temperature," *IEEE Journal of Quantum Electronics* **48**(9), 1107–1112 (2012).

[8] Hsieh, D. H., Tzou, A. J., Kao, T. S., Lai, F. I., Lin, D. W., Lin, B. C., Lu, T. C., Lai, W. C., Chen, C. H., and Kuo, H. C., "Improved carrier injection in GaN-based VCSEL via AlGaN/GaN multiple quantum barrier electron blocking layer," *Opt. Express* **23**(21), 27145–27151 (2015).

[9] Leonard, J. T., Young, E. C., Yonkee, B. P., Cohen, D. A., Margalith, T., DenBaars, S. P., Speck, J. S., and Nakamura, S., "Demonstration of a III-nitride vertical-cavity surface-emitting laser with a III-nitride tunnel junction intracavity contact," *Applied Physics Letters* **107**(9), 091105 (2015).

[10] Hamaguchi, T., Fuutagawa, N., Izumi, S., Murayama, M., and Narui, H., "Milliwatt-class GaN-based blue vertical-cavity surface-emitting lasers fabricated by epitaxial lateral overgrowth," *Physica Status Solidi (a)* **213**(5), 1170–1176 (2016).

[11] Ikeyama, K., Kozuka, Y., Matsui, K., Yoshida, S., Akagi, T., Akatsuka, Y., Koide, N., Takeuchi, T., Kamiyama, S., Iwaya, M., and Akasaki, I., "Room-temperature continuous-wave operation of GaN-based vertical-cavity surface-emitting lasers with n-type conducting AlInN/GaN distributed Bragg reflectors," *Applied Physics Express* **9**(10), 102101 (2016).

[12] Weng, G., Mei, Y., Liu, J., Hofmann, W., Ying, L., Zhang, J., Bu, Y., Li, Z., Yang, H., and Zhang, B., "Low threshold continuous-wave lasing of yellow-green InGaN-QD vertical-cavity surface-emitting lasers," *Opt. Express* **24**(14), 15546–15553 (2016).

[13] Vurgaftman, I. and Meyer, J. R., "Band parameters for nitrogen-containing semiconductors," *Journal of Applied Physics* **94**(6), 3675–3696 (2003).

[14] Lu, T.-C., Chen, S.-W., Wu, T.-T., Tu, P.-M., Chen, C.-K., Chen, C.-H., Li, Z.-Y., Kuo, H.-C., and Wang, S.-C., "Continuous wave operation of current injected GaN vertical cavity surface emitting lasers at room temperature," *Applied Physics Letters* **97**(7), 071114 (2010).

[15] Lin, B. C., Chang, Y. A., Chen, K. J., Chiu, C. H., Li, Z. Y., Lan, Y. P., Lin, C. C., Lee, P. T., Kuo, Y. K., Shih, M. H., Kuo, H. C., Lu, T. C., and Wang, S. C., "Design and fabrication of a InGaN vertical-cavity surface-emitting laser with a composition-graded electron-blocking layer," *Laser Physics Letters* **11**(8), 085002 (2014).

[16] Furuta, T., Matsui, K., Horikawa, K., Ikeyama, K., Kozuka, Y., Yoshida, S., Akagi, T., Takeuchi, T., Kamiyama, S., Iwaya, M., and Akasaki, I., "Room-temperature CW operation of a nitride-based vertical-cavity surface-emitting laser using thick GaInN quantum wells," *Japanese Journal of Applied Physics* **55**, 05FJ11 (2016).

[17] Matsui, K., Kozuka, Y., Ikeyama, K., Horikawa, K., Furuta, T., Akagi, T., Takeuchi, T., Kamiyama, S., Iwaya, M., and Akasaki, I., "GaN-based vertical cavity surface emitting lasers with periodic gain structures," *Japanese Journal of Applied Physics* **55**, 05FJ08 (2016).

[18] Arita, M., Nishioka, M., and Arakawa, Y., "InGaN vertical microcavity LEDs with a Si-doped AlGaN/GaN distributed Bragg reflector," *Physica Status Solidi (a)* **194**(2), 403–406 (2002).

[19] Ive, T., Brandt, O., Kostial, H., Hesjedal, T., Ramsteiner, M., and Ploog, K. H., "Crack-free and conductive Si-doped AlN/GaN distributed Bragg reflectors grown on 6H-SiC(0001)," *Applied Physics Letters* **85**(11), 1970–1972 (2004).

[20] Figge, S., Dartsch, H., Aschenbrenner, T., Kruse, C., and Hommel, D., "Distributed Bragg reflectors in comparison to RUGATE and nested super lattices growth, reflectivity, and conductivity," *Physica Status Solidi (c)* **5**(6), 1839–1842 (2008).

[21] Liu, Y.-S., Haq, A. F. M. S., Kao, T.-T., Mehta, K., Shen, S.-C., Detchprohm, T., Yoder, P. D., Dupuis, R. D., Xie, H., and Ponce, F. A., "Electrically conducting n-type AlGaN/GaN distributed Bragg reflectors grown by metalorganic chemical vapor deposition," *Journal of Crystal Growth* **443**, 81 – 84 (2016).

[22] Yoshida, S., Ikeyama, K., Yasuda, T., Furuta, T., Takeuchi, T., Iwaya, M., Kamiyama, S., and Akasaki, I., "Electron and hole accumulations at GaN/AlInN/GaN interfaces and conductive n-type AlInN/GaN distributed Bragg reflectors," *Japanese Journal of Applied Physics* **55**, 05FD10 (2016).

[23] Adolph, D., Zamani, R. R., Dick, K. A., and Ive, T., "Hybrid ZnO/GaN distributed Bragg reflectors grown by plasma-assisted molecular beam epitaxy," *APL Mater.* **4**(8), 086106 (2016).

[24] Park, Y. S. and Schneider, J. R., "Index of refraction of ZnO," *Journal of Applied Physics* **39**(7), 3049–3052 (1968).

[25] Brunner, D., Angerer, H., Bustarret, E., Freudenberg, F., Hpler, R., Dimitrov, R., Ambacher, O., and Stutzmann, M., "Optical constants of epitaxial AlGaN films and their temperature dependence," *Journal of Applied Physics* **82**(10), 5090–5096 (1997).

[26] Karzel, H., Potzel, W., Köfferlein, M., Schiessl, W., Steiner, M., Hiller, U., Kalvius, G. M., Mitchell, D. W., Das, T. P., Blaha, P., Schwarz, K., and Pasternak, M. P., "Lattice dynamics and hyperfine interactions in ZnO and ZnSe at high external pressures," *Phys. Rev. B* **53**, 11425–11438 (1996).

[27] Xu, H. Y., Liu, Y. C., Liu, Y. X., Xu, C. S., Shao, C. L., and Mu, R., "Ultraviolet electroluminescence from p-GaN/i-ZnO/n-ZnO heterojunction light-emitting diodes," *Applied Physics B* **80**(7), 871–874 (2005).

[28] Ben-Yaacov, T., Ive, T., Van de Walle, C. G., Mishra, U. K., Speck, J. S., and Denbaars, S. P., "Properties of In-doped ZnO films grown by metalorganic chemical vapor deposition on GaN(0001) templates," *Journal of Electronic Materials* **39**(5), 608–611 (2010).

[29] Hanada, T., "Basic properties of ZnO, GaN, and related materials," in [*Oxide and Nitride Semiconductors: Processing, Properties, and Applications*], Yao, T. and Hong, S.-K., eds., 1–19, Springer Berlin Heidelberg, Berlin, Heidelberg (2009).

[30] Bernardini, F., Fiorentini, V., and Vanderbilt, D., "Spontaneous polarization and piezoelectric constants of III-V nitrides," *Phys. Rev. B* **56**, R10024–R10027 (1997).

[31] Bateman, T. B., "Elastic moduli of single-crystal zinc oxide," *Journal of Applied Physics* **33**(11), 3309–3312 (1962).